



# Development of the rain/no-rain classification and the SLH algorithm over the Tibetan Plateau

Munehisa K. Yamamoto<sup>1</sup>, \*Shoichi, Shige<sup>1</sup>, and Ippei Tanaka<sup>2</sup>

1: Graduate School of Science, Kyoto University

2: Faculty of Science, Kyoto University



## Improvement of rain/no-rain classification method for microwave radiometers

IEEE Geosci. Remote Sens. Lett., 14, 626–630. (2017)

### Introduction

Tropospheric heating and cooling over the Tibetan Plateau play an important role in the progress of the Asian summer monsoon. Precipitation is a major factor influencing surface conditions such as vegetation and snow cover, which also interact with convective cloud and precipitation systems. Therefore, precise estimation of precipitation and latent heating are needed. Giving the plateau's high altitude, complex topography, and lack of surface observation networks, satellite measurements represent a powerful tool for estimating area-wide precipitation amounts for the Plateau. Several rainfall retrieval algorithms for microwave radiometers have been developed, meanwhile previous studies mentioned poor consistency over the Plateau. **This study identifies the causes of the deterioration of the Global Satellite Mapping of Precipitation rain detection over the Plateau during the summer monsoon season.**

### Data

#### Period:

May 5–September 19, 1998 (GAME-Tibet IOP)

#### Area:

30.6°–32.2°N, 91°–93°E (displayed in Fig. 2)

#### Data:

**TRMM PR:** Near surface rainfall

**TMI:** Tb at 21 and 85 GHz

**DMSP SSM/ (F14):** Tb at 23 and 85 GHz

**GSMaP:** rainfall estimated from TMI and SSM/I by algorithm version 6 (referred as GSMaP1).

**GPROF:** rainfall estimated from TMI

**NASDA X-band Doppler radar** (31.4 ° N, 91.9 ° E, 4548 m; 9.4 GHz, every 10-min at a 64 km range): Z converted into 1- and 0.5-km horizontal and vertical resolutions.

**AWS at MS3478** (31.9 ° N, 91.7 ° E, 5063 m above sea level in a wet glass landrainfall): soil moisture at 3 levels, air temperature, and rainfall

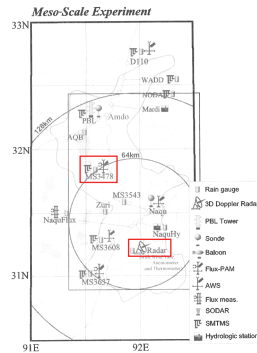


Fig. 1. Map of the mesoscale observation area for GAME-Tibet. Circles indicate the observation area of the Doppler radar. The rectangle indicates the sampling area of TRMM PR data (After Shimizu et al. 2001, JMSJ).

### Rain undetected case (June 17, 1998)

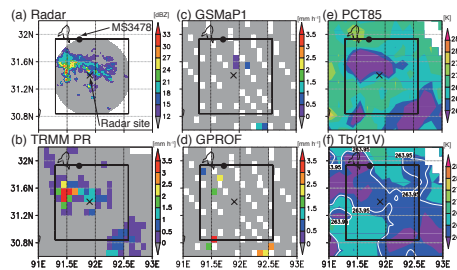


Fig. 3. Horizontal distributions of (a) radar reflectivity factor at 2 km above the surface from the NASDA radar, surface rainfall from (b) near surface rainfall from TRMM PR, (c) GSMaP1, (d) GPROF, (e) PCT85, and (f) Tb(21V) from TRMM TMI with white contour at 263.95 K. The TRMM orbit number and overpass time are 03182 and 2208 LT on June 17, 1998, respectively. The scan time for the radar is 2210 LT. Black dots denote the surface observation site MS3478, and the X-marker shows the radar site.

### Replacement of satellite measured ε

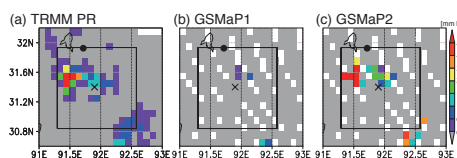


Fig. 5. Horizontal distributions of surface rainfall from (a) near surface rainfall from TRMM PR (b) GSMaP1, and (c) GSMaP2.

After ε is replaced with values from a monthly mean satellite observation based land surface emissivity database (GSMaP2), rainfall detection is improved (Fig. 5). In addition, it is suggested that a **database of RNCs should also consider diurnal variations in Tb(21 V) and Tb(23 V) due to large diurnal differences over the Plateau** (Table 1).

### Rain-no-rain classification (RNC) method (Seto et al. 2005)

#### Scattering Index (SI)

$SI = Tb(85 V)_{obs} - Tb(85 V)_{no-rain}$   
 $Tb(85 V)_{obs} = a + b \times Tb(21 V)_{obs}$   
where a and b are calculated in a  $0.25^\circ \times 0.25^\circ$  latitude-longitude grid for each month

$Tb(85 V)_{obs} < Tb(85 V)_{SI} = a + b \times Tb(21 V)_{obs} - k_0 \times \sigma_{e}$   
 $k_0$  represents an empirically set global constant parameter (=3.5).

#### Snow cover screening

$Tb(21 V) < 260.0$  K or surface temp. (Ts) < 273.2 K

$T_s = Tb(21 V) / \epsilon$ ,  $\epsilon = 0.966$  for > 1 km altitude

$Tb(21 V) < 273.2 \times \epsilon = 263.9$  K

$Tb(85 V)_{snow} = a + b \times 263.9 - k_0 \times \sigma_{e}$

Observed brightness temperature (Tb) at 21 (23) GHz from TMI and SSM/I (Tb(21 V) and Tb(23 V)), and surface emissivity (ε) was substituted for surface temperatures (Ts) to exclude areas of low Ts as snow cover because it is difficult to distinguish between the scattering signals of precipitation and snow cover.

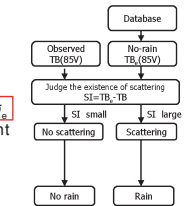


Fig. 2. Schematic of RNC method for GSMaP (after Seto et al. 2005, JAM).

### Progress of the Asian summer monsoon

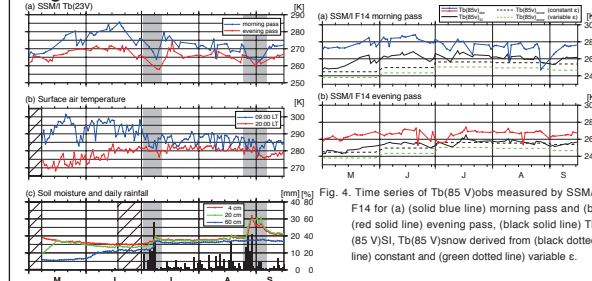


Fig. 4. Time series of (a) Tb(23 V) measured by SSM/I F14 for (blue line) morning and (red line) evening passes, (b) surface air temperature at (blue line) 0900 LT and (red) 2000 LT, (c) (solid lines) soil moisture at (red line) 4 cm, (green line) 20 cm, and (blue line) 60 cm, and (bar) daily rainfall measured by ground instruments at MS3478 from May 1 to September 15, 1998. Hatched areas indicate no observation for rain. Gray shaded areas indicate focus periods.

A constant value of ε was used for calculating  $Tb(85 V)_{snow}$  (dashed black line in Fig. 4). Days classified as having snow cover, when  $Tb(85 V)_{SI}$  was less than  $Tb(85 V)_{snow}$ , were July 10 and August 26 to September 3 for the morning pass. Using the **monthly mean satellite measured ε** (dashed green line in Fig. 4), there were **no days when  $Tb(85 V)_{SI}$  was less than  $Tb(85 V)_{snow}$  for both morning and evening passes.**

### Improvement of verification score

	GPROF	GSMaP1	GSMaP2
POD (day)	0.619 (0.525)	0.522 (0.468)	0.672 (0.704)
(night)	0.601 (0.524)	0.288 (0.411)	0.599 (0.873)
FAR (day)	0.648 (0.598)	0.548 (0.541)	0.559 (0.584)
(night)	0.711 (0.720)	0.572 (0.572)	0.558 (0.674)
CSI (day)	0.289 (0.295)	0.320 (0.301)	0.363 (0.354)
(night)	0.243 (0.223)	0.208 (0.265)	0.341 (0.311)

Table 1. The verification scores are for areas within the study area with rainfall of more than 0.5 mm h<sup>-1</sup> for JJA in 1998–2000 for (day) 06–18 LT and (night) 18–06 LT. Numbers in parentheses are those within the Andes Mountains for DJF.

## Development of the Spectral Latent Heating (SLH) algorithm

### Introduction

The spectral latent heating (SLH) algorithm has been developed using vertical profiles of precipitation from TRMM Precipitation Radar. However, SLH is not estimated over the highland areas including the Plateau and mid-latitude in winter since the characteristics of the precipitation system are greatly different from tropics. In order to develop a look-up table for SLH estimation over the highland area, a case study for precipitation system over the Plateau on 6 July, 2013 is carried out using the Weather Research and Forecasting (WRF) Model and a satellite data simulator.

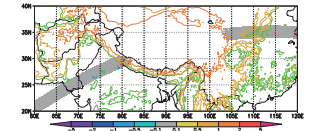


Fig. 6. Topography (contour) at (green) 0.5, (dark yellow) 1, and (orange) 3 km and horizontal distribution of latent heating at 5 km from the surface.

### Data and data processing

#### WRF 3.8

Input: NCEP FNL 1° × 1°, 26 layers, 6 hourly

Output: standard output + microphysics latent heating (h<sub>diabatic</sub>)

#### SDSU 2.1.4

Input: WRF output in d02, 36 levels (every 250 m)

Output: Synthetic measurements of TRMM PR (13.8 GHz, corrected Z)

Domain	d01	d02	d03
Horizontal grids	150 × 150	151 × 151	151 × 151
Grid spacing	27 km	9 km	3 km
Integration time	0–24	0–24	0–24
Planetary boundary layer	YSU	YSU	YSU
Microphysics	WSM6	WSM6	WSM6
Cumulus parameterization	Grell-3	Grell-3	Not used
Longwave Radiation	Dudhia	Dudhia	Dudhia
Shortwave Radiation	RRTM	RRTM	RRTM

### Case study (July 6, 2013)

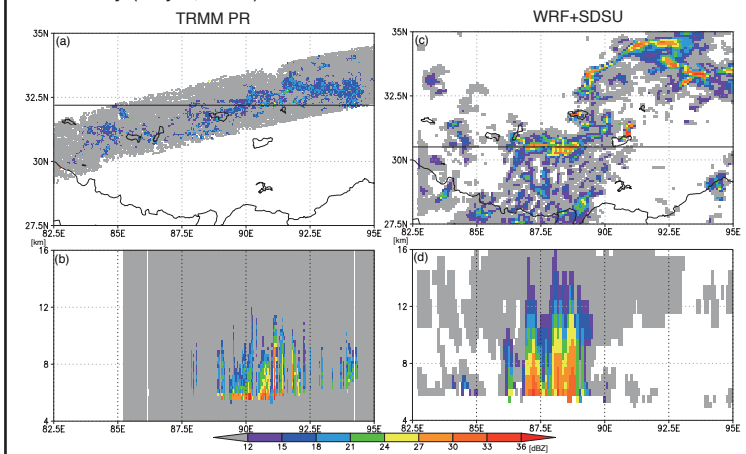


Fig. 7. (a) Horizontal distributions of Ze at 7 km above sea level and (b) vertical distributions of Ze at 32.5°N from TRMM PR. The TRMM orbit number and overpass time are 09089 and 2058 UTC on July 6, 2013, respectively. (c) and (d) The same as (a) and (b) except from WRF and SDSU simulation at 21 UTC (initial time is 00 UTC), and at 30.5°N for (d).

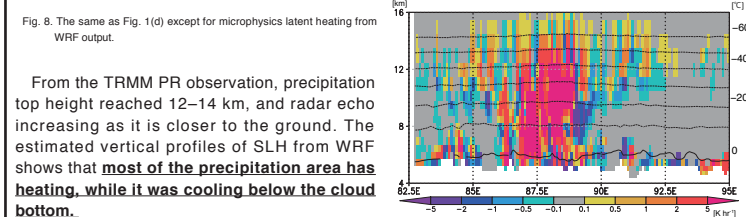


Fig. 8. The same as Fig. 1(d) except for microphysics latent heating from WRF output.

From the TRMM PR observation, precipitation top height reached 12–14 km, and radar echo increasing as it is closer to the ground. The estimated vertical profiles of SLH from WRF shows that **most of the precipitation area has heating, while it was cooling below the cloud bottom.**